Downloaded from orbit.dtu.dk on: Aug 27, 2022

DTU Library

Insights into the carbon balance for CO2 electroreduction on Cu using gas diffusion electrode reactor designs

Ma, Ming; Clark, Ezra L.; Therkildsen, Kasper T.; Dalsgaard, Sebastian; Chorkendorff, Ib; Seger, Brian

Published in:
Energy and Environmental Science

Link to article, DOI:
10.1039/d0ee00047g

Publication date:
2020

Document Version
Publisher's PDF, also known as Version of record

Link back to DTU Orbit

Citation (APA):
Ma, M., Clark, E. L., Therkildsen, K. T., Dalsgaard, S., Chorkendorff, I., & Seger, B. (2020). Insights into the carbon balance for CO_2 electroreduction on Cu using gas diffusion electrode reactor designs. *Energy and Environmental Science*, *13*(3), 977-985. https://doi.org/10.1039/d0ee00047g

General rights
Copyright and moral rights for the publications made accessible in the public portal are retained by the authors and/or other copyright owners and it is a condition of accessing publications that users recognise and abide by the legal requirements associated with these rights.

- Users may download and print one copy of any publication from the public portal for the purpose of private study or research.
- You may not further distribute the material or use it for any profit-making activity or commercial gain
- You may freely distribute the URL identifying the publication in the public portal

If you believe that this document breaches copyright please contact us providing details, and we will remove access to the work immediately and investigate your claim.

Energy & Environmental Science

ROYAL SOCIETY OF CHEMISTRY

PAPER

View Article Online
View Journal | View Issue

Check for updates

Cite this: *Energy Environ. Sci.*, 2020, **13**, 977

Insights into the carbon balance for CO_2 electroreduction on Cu using gas diffusion electrode reactor designs†

Ming Ma,[a] Ezra L. Clark,[a] Kasper T. Therkildsen,[b] Sebastian Dalsgaard,[a] Ib Chorkendorff[a] and Brian Seger*[a]

Received 6th January 2020,
Accepted 12th February 2020

DOI: 10.1039/d0ee00047g

rsc.li/ees

In this work, the carbon balance during high-rate CO_2 reduction in flow electrolyzers was rigorously analyzed. The CO_2 consumption at gas-diffusion electrodes due to electrochemical conversion and reaction with OH^- at the electrode/electrolyte interface leads to a substantial reduction in the volumetric flowrate of gas flow out of the electrolyzer, especially when highly concentrated alkaline electrolytes and elevated current densities are utilized, which is primarily due to an elevated pH at cathode/electrolyte interface. Without considering the CO_2 consumption, the faradaic efficiencies for major gas products could be significantly overestimated during high current density CO_2 reduction conditions, particularly in the case of high pH electrolyte. In addition, a detailed carbon balance path is elucidated *via* a two-step procedure of CO_2 reaction with OH^- at the cathode/electrolyte interface and subsequent CO_2 generation at the anode/electrolyte interface caused by a relatively low pH in the vicinity of the anode. Based on the proposed two-step carbon balance path, a systematic exploration of gases released in the anolyte reveals the transformation of a HCO_3^- or OH^- catholyte to a CO_3^{2-} catholyte, which was further confirmed by pH measurements.

Broader context

Electrochemical CO_2 reduction allows for a sustainable path to convert CO_2 into some of the carbonaceous species we need in everyday life such as plastics, composites, solvents, *etc.* The rapidly decreasing price of solar and wind based renewable electricity is pushing this field forward quite rapidly. However, in the quest to convert fundamental scientific discoveries into commercially relevant devices, we need to ensure that there are no unintended consequences. This work shows a clear carbon balance path using a typical anion exchange membrane with various electrolytes. We demonstrate that ~70% of the consumed CO_2 is captured from cathode/catholyte interface and released from the anolyte, which is significantly higher than that, which is actually converted to products (*i.e.* only ~30% of consumed CO_2 is involved in product formation). In addition, this discovery means that the gas flowrate out of the reactor will be reduced, thus having a significant effect on reported selectivity of gas products if CO_2 consumption is not properly accounted for. In basic conditions and at low CO_2 inlet flow rates, we show that gaseous CO_2 reduction products can be overestimated by 64% if the gas outlet flow is not properly accounted for.

Introduction

The electrochemical conversion of CO_2 into fuels and valuable chemicals under mild conditions has gained significant interest as an attractive route for the storage of intermittent renewable energy and the utilization of the captured CO_2.[1–8] Over the past few decades, the focus of most CO_2 reduction research has concentrated on the development of selective, efficient and stable electrocatalytsts using traditional H-cell reactors filled with CO_2-saturated aqueous solutions.[9–12] Researchers have substantially reduced the overpotentials required for driving selective CO_2 reduction *via* tuning morphologies,[13,14] compositions,[15] crystal facets[16,17] and oxidation states of catalysts.[18] Although impressive progress has been made on improving the catalytic performance, low CO_2 solubility in aqueous electrolyte and the thick mass-transfer boundary layer (>50 μm) in H-cell type reactors lead to poor CO_2 mass transport to the surface of the catalysts,[19,20] which significantly limits the current densities, preventing the potential for practical applications.

To overcome the mass transport limitations, many attempts have focused on CO_2 reduction in flow-cell reactors with gas-diffusion electrodes (GDEs), which can offer a dramatically thinner mass-transfer boundary layer (~50 nm) that is a 3-order of magnitude decrease compared to that in H-cell reactors.[19–21]

[a] *Surface Physics and Catalysis (SurfCat) Section, Department of Physics, Technical University of Denmark, 2800 Kgs. Lyngby, Denmark. E-mail: brse@fysik.dtu.dk*
[b] *Siemens A/S, RC-DK SI, Diplomvej 378, 2800 Kgs. Lyngby, Denmark*

† Electronic supplementary information (ESI) available. See DOI: 10.1039/d0ee00047g

Published on 12 February 2020. Downloaded by DTU Library on 11/20/2020 11:30:33 AM.

Published on 12 February 2020. Downloaded by DTU Library on 11/20/2020 11:30:33 AM.

Based on flow-cell configurations, the electrocatalytic conversion of CO_2 has been widely performed in highly concentrated neutral solutions (such as $KHCO_3$), demonstrating commercially-relevant current densities (>100 mA cm^{-2}).[22–26] To further improve performance of CO_2 reduction electrolysis, highly concentrated KOH solutions are becoming commonly employed in GDE-type flow electrolyzers, owing to the high conductivity of OH^- and the reduction of activation energy barriers for CO_2 reduction influenced by OH^-.[21,26–31] However, it is well known that OH^- can react with CO_2 to form HCO_3^- or CO_3^{2-} according to the reactions below:

$$OH^- + CO_2 \leftrightarrow HCO_3^- \ (pK_a = 7.8^*) \quad (1)$$

$$OH^- + HCO_3^- \leftrightarrow CO_3^{2-} + H_2O \ (pK_a = 10.3) \quad (2)$$

*This is at a CO_2 partial pressure of 1 bar in 1 M HCO_3^-.

These reactions inherently lead to a change of electrolytes (anion species) over time, which has the potential to influence catalytic activity of CO_2 reduction. Recently, a slight decrease in current density was discovered during high-rate CO_2 reduction in 1 M KOH electrolyte, which was attributed to the anion composition changing from OH^- to CO_3^{2-}.[24] However, direct evidence of the anion species transformation during high-rate CO_2 reduction is still lacking.

In addition, there is a much more practical issue that comes with operating CO_2 reduction in basic conditions. Gaseous CO_2 reduction products are almost always quantified by measuring a concentration (*e.g. via* a GC) and monitoring the gas flow, as indicated in eqn (S2) (ESI†) for the catalytic selectivity calculation. While the incoming CO_2 flow can easily be measured by thermal mass flowmeters, variation in product streams (a mixture of different gases) coming out of the reactor limits the available techniques for measuring outlet flows (variations in thermal conductivity and viscosity give issues with many measuring techniques). At neutral pH electrolytes and low current densities, it is reasonable to approximate that outlet flows are equivalent to inlet flows since conversion rates are low (such as most cases involving H-cell set-ups). However, basic solutions with the ability of capturing CO_2 *via* reaction with OH^- can significantly change the outlet flowrates. In addition, CO_2 conversion into C_2 gas products and liquid products at high reaction rates (*i.e.* high current densities) also affects the gas outlet flowrates. Thus, the measurement of outlet gas flow in high-rate CO_2 reduction plays an important role in the calculation of faradaic efficiency (FE) of gas products. However, currently the majority of work in high-rate CO_2 electroreduction[21–23,28,31–36] have not explicitly stated that their faradaic efficiency calculations were based on the outlet gas flow from their reactor (with the exception of a few works on CO_2 reduction to CO[37,38]). While lack of experimental details prevent understanding exactly how these works were employed, the results of the aforementioned works could be inadvertently distorted if they did use inlet gas flowrates to evaluate catalytic selectivity and activity. Therefore, to ensure accuracy of reported results in GDEs-type electrolyzers, it is critical to fundamentally understand the carbon balance and benchmark the evaluation of the catalytic selectivity (or FE) at high current densities.

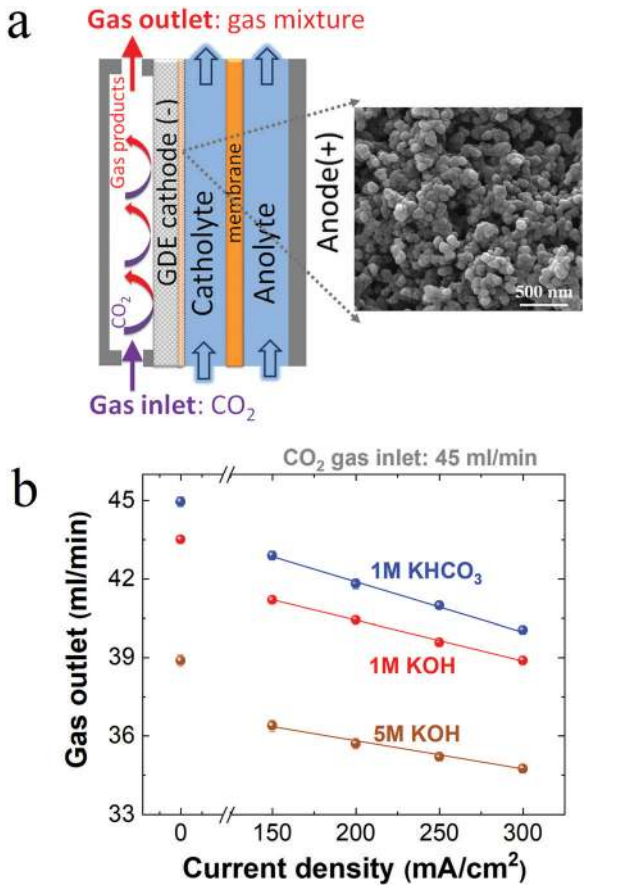

Fig. 1 (a) Schematic illustration of three-compartment flow electrolyzers, and SEM image of Cu catalysts on GDEs. (b) Gas outlet flowrates from gas chamber after CO_2 reduction in 1 M $KHCO_3$, 1 M KOH and 5 M KOH, respectively.

Herein, we demonstrate that CO_2 consumption *via* the reaction with OH^- in flow electrolyzers (Fig. 1a) can significantly reduce the total flowrate of gas outlet after electrolysis, especially in highly concentrated alkaline solutions and at elevated current densities. This study also shows how the CO_2 consumption can affect the evaluation of CO_2 reduction results and how electrolyte speciation dynamically changes at high current densities. In addition, this study provides new insights into the carbon balance of flow electrolyzers *via* systemically exploring carbon paths and the transformation of ion species in both the catholyte and the anolyte.

Experimental methods

Fabrication and characterization of Cu catalysts

To obtain high purity Cu electrocatalyst layers on GDEs, the Cu catalysts were deposited by magnetron sputtering at an argon pressure of 2 mTorr. Fig. 1a shows a typical scanning electron microscope image (SEM) of the Cu catalysts coated on top of microporous carbon layers. In addition, the cross-sectional SEM image (Fig. S1, ESI†) indicates that the Cu deposition rate was $\sim$4 nm min^{-1}. Using this technique, $\sim$70 nm thick Cu catalyst layers on GDEs was synthesized. To identify the phase

 This journal is © The Royal Society of Chemistry 2020

Published on 12 February 2020. Downloaded by DTU Library on 11/20/2020 11:30:33 AM.

of Cu catalysts, X-ray diffraction (XRD) measurements were conducted. The XRD patterns (Fig. S4, ESI†) show the PTFE[39] and carbon peaks derived from GDE substrates as well as the (111), (200), and (211) Cu peaks with the dominant (111) peak.

Electrocatalytic CO_2 reduction

Electrochemical CO_2 reduction was performed in a three-compartment flow electrolyzer, consisting of catholyte and anolyte flow compartments which are separated by an anion exchange membrane (AEM), and a gas compartment which allows gases to flow in and out of the reactor, as shown in Fig. 1a. The cathodic gas flow compartment was continuously fed with CO_2 at a constant flow rate (45 ml min^{-1}), and a fraction of the CO_2 was converted into gas products, which directly vented into the gas-sampling loop of a gas chromatograph (GC) for periodic quantification (Fig. S5, ESI†). Liquid-phase products formed during the CO_2 reduction were diluted in the given reservoir (catholyte and anolyte), and recycled until the test was finished. After completion of electrolysis, liquid-phase products were identified and quantified *via* high-performance liquid chromatography (HPLC).

Results and discussion

To verify the variation in gas flowrate between reactor gas inlet and outlet, a volumetric flowmeter was used to monitor the outlet flow of the reactor (Fig. S5, ESI†). Fig. 1b shows the outlet flowrate as a function of current density (J) in 1 M $KHCO_3$, 1 M KOH and 5 M KOH, respectively. Without electrolysis (*i.e.* J = 0 mA cm^{-2}), there is no obvious discrepancy in the flowrate between gas inlet and outlet in 1 M $KHCO_3$. In contrast, a clear decrease in the outlet flowrate was observed upon increasing the alkalinity of the electrolyte (J = 0 mA cm^{-2}), which stems from the enhanced CO_2 consumption rate through the reaction of CO_2 and OH^- in high pH solutions (*via* eqn (1) and (2)). As current densities increased, outlet flow gradually decreased in all the electrolytes, which corresponds to a gradual enhancement in consumption rate of CO_2.

This increase in CO_2 consumption rate at elevated current densities can be ascribed to two reasons, (i) an enhanced CO_2 reduction rate and (ii) local pH effects. Specifically, higher current densities correspond to an increased conversion rate of CO_2 into gaseous (C_2) and liquid products, which results in an increase in CO_2 consumption, partially contributing to a variation in outlet flow. In addition, there is an enhanced OH^- generation rate at the electrode/electrolyte interface upon increasing current densities *via* cathodic reactions (hydroxyl groups generation rate is linearly correlated with current densities based on eqn (S3)–(S9), ESI†), which creates a high local pH near the surface of the catalyst, thus further favoring additional CO_2 consumption *via* eqn (1) and (2). The current induced pH variations near the surface of the catalyst (and concomitant CO_2 consumption) should be most obvious in moderate pH solutions. Thus, as expected, a careful analysis of variations in gas outlet flowrates as a function of current density reveals a larger decrease in outlet gas flowrates with increasing current densities in moderate pH electrolytes (slope value in Fig. S6, ESI:† 1 M $KHCO_3$ > 1 M KOH > 5 M KOH). All the above findings imply that high-rate CO_2 reduction results in substantial CO_2 consumption *via* a local pH effect (high local pH) and high CO_2 conversion rate to liquid and C_2 gas products, thus varying the outlet flowrate. This flow variation is particularly apparent in the case of highly concentrated alkaline solutions.

It should be noted that the CO_2 consumption rate (flowrate alteration) is also linked to GDE surface area used in flow-electrolyzers and mass transport properties that are potentially influenced by the type of GDEs, reactor design, CO_2 flowrate, catholyte flow, *etc.* For simplification, all these parameters were kept constant in this work, with the exception of later section in which the effects of CO_2 inlet flowrate were investigated.

The faradaic efficiencies of the gas products formed over Cu catalysts in different electrolytes were plotted at various current densities with and without considering the changes of gas outlet flowrates (Fig. 2). As noted in Fig. 1, the gaseous product distribution is primarily ethylene across all tested current densities, with small amounts of H_2 and CO and only trace amounts of CH_4. If one would not have considered CO_2 consumption (*i.e.* columns with dashed line in Fig. 2a–c), it seems as if the faradaic efficiency for C_2H_4 had a slight improvement from 1 M $KHCO_3$ to 1 M KOH, and then significantly increased for 5 M KOH. However, there appears to be no significant variation in ethylene across all different electrolytes and current densities ranges after considering CO_2 consumption and concomitant change in outlet flow (*i.e.* solid columns). In addition, Hori *et al.* has demonstrated that formation rates of C_2 products (C_2H_4 and ethanol) are independent of the pH of electrolyte, but are correlated with electrode potential.[40] Here, we also found that the role of bulk pH may be minimal in affecting ethylene selectivity for CO_2 reduction at high current densities after taking into consideration of the outlet flow variation (at roughly identical potentials ranges, as shown in Tables S3 and S4, ESI†). Thus, the error introduced by disregarding CO_2 consumption could lead to the misunderstanding of trends in catalytic activity and erroneous conclusions about superior operating conditions.

The discrepancy in the faradaic efficiency for C_2H_4 (major gas product) with and without considering CO_2 consumption became larger at higher current densities for the same electrolyte, as shown in Fig. 2d. Notably, an overestimated faradaic efficiency of 12% for C_2H_4 formation was discovered in 5 M KOH without considering the CO_2 consumption at 300 mA cm^{-2}, which is much higher compared to those in 1 M KOH (7%) and 1 M $KHCO_3$ (5.9%) under identical conditions (Fig. 2d). This result indicates that faradaic efficiencies for major gas products during high-rate CO_2 reduction in flow electrolyzers could be significantly overestimated without consideration of CO_2 consumption (using uncorrected gas flowrate), especially for highly concentrated alkaline electrolytes.

In addition to gaseous products, ethanol was observed as a major liquid product across all current densities in 1 M $KHCO_3$ and 1 M KOH, along with small amounts of *n*-propanol, formate and acetate as well as only trace amounts of allyl alcohol, acetaldehyde, glycolaldehyde and ethylene glycol (Fig. 3). Of particular note, the

Published on 12 February 2020. Downloaded by DTU Library on 11/20/2020 11:30:33 AM.

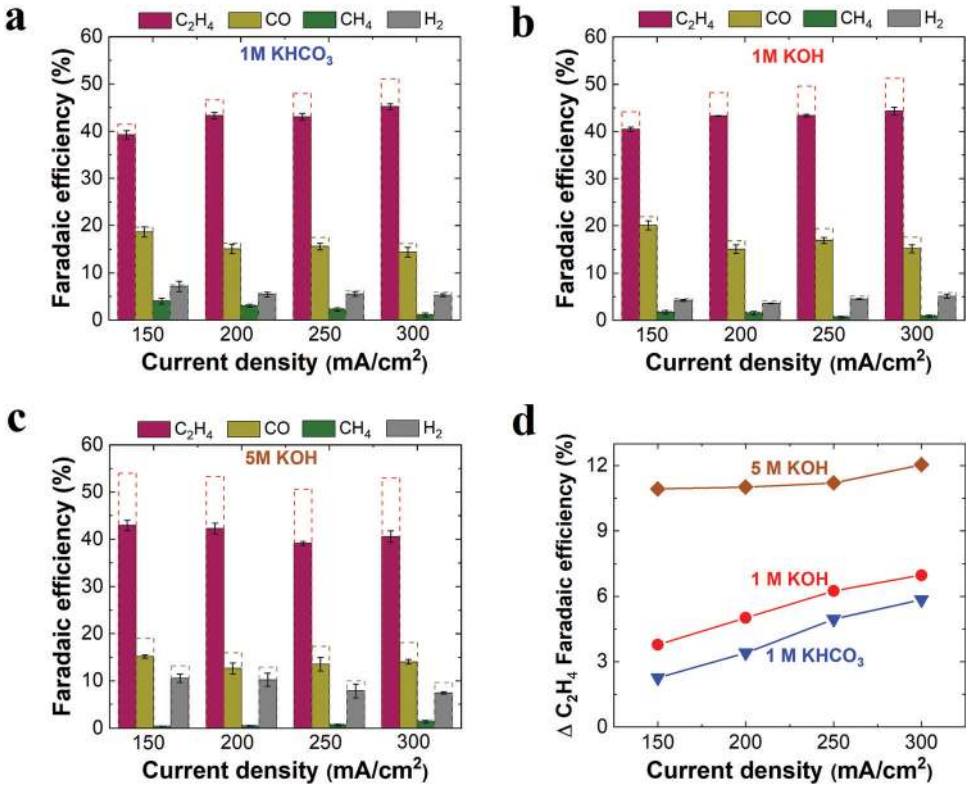

Fig. 2 Comparison of the electrocatalytic performance of Cu-coated on GDEs in different electrolyte. The faradaic efficiencies for gas products in 1 M $KHCO_3$ (a), 1 M KOH (b) and 5 M KOH (c) at various current densities, based on corrected and uncorrected gas flowrate, respectively (columns with dash line show the faradaic efficiency calculated using uncorrected gas flowrate without considering CO_2 consumption). (d) Difference in C_2H_4 faradaic efficiency with and without the consideration of CO_2 consumption. The difference values were obtained by comparing C_2H_4 faradaic efficiency in dash lines with related solid lines in (a)—(c).

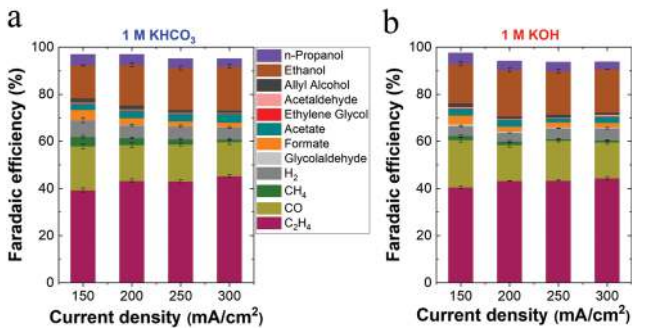

Fig. 3 Faradaic efficiencies for all detected gas and liquid products in 1 M $KHCO_3$ (a) and 1 M KOH (b) at various current densities.

faradaic efficiencies of liquid products were obtained based on analysis of both catholyte and anolyte since it was discovered that some liquid products crossed over from the catholyte to the anolyte *via* the AEM (Fig. S16, ESI†). Specifically, while the crossover ratio of most of uncharged products such as ethanol and *n*-propanol were very small (almost negligible), the anionic CO_2 reduction products such as formate and acetate experienced substantial crossover by electromigration across all current densities (Fig. S17, ESI†), which is consistent with a previous report.[41] In addition, a disproportionate amount of acetaldehyde crossed over to the anolyte (the crossover ratio of acetaldehyde was relatively high in Fig. S17a, ESI†). With near 20% ethanol FE (dominant liquid product in Fig. 3), this disproportionate acetaldehyde crossover indicates CO_2 reduction potentially produced a significantly higher amount of acetaldehyde at the cathode initially, but most of acetaldehyde was further reduced to ethanol as the catholyte was continually recycled during electrolysis.[42]

Effect of CO_2 inlet flowrate

We also investigted the influence of CO_2 inlet flowrate on the evaluation of faradaic efficiencies for major gas products in flow electrolyzers with and without the consideration of CO_2 consumption in 1 M KOH electrolyte at 300 mA cm^{-2}. If one would not have considered the CO_2 consumption, it appears as if the C_2H_4 faradaic efficiency dramatically enhanced upon decreasing CO_2 inlet flow from 45 ml min^{-1} to 15 ml min^{-1}, as shown in Fig. 4a (columns with dash line). However, once CO_2 consumption is considered and the proper outlet flow rates are used, these results show that CO_2 inlet flowrate had only a small effect on faradaic efficiencies for all the major gas products. The only notable difference is that there was a slight decrease in CO formation and a slight increase in ethylene production at low flowrates. This observation is likely due to that the significantly increased CO partial pressure in the reactor at low flow (*i.e.* CO concentration: 1.7% at 45 ml min^{-1} and 5.5% at 15 ml min^{-1}, as shown in Table S7, ESI†) allows for more CO conversion to ethylene.

 This journal is © The Royal Society of Chemistry 2020

Published on 12 February 2020. Downloaded by DTU Library on 11/20/2020 11:30:33 AM.

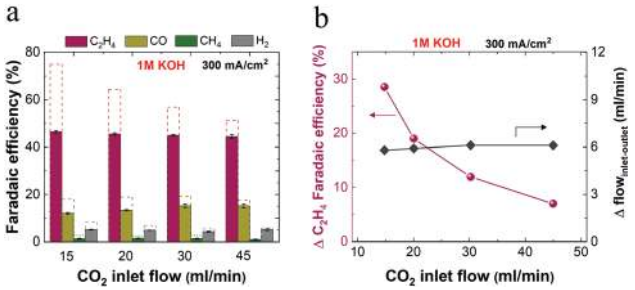

Fig. 4 (a) Faradaic efficiencies for gas products in 1 M KOH with and without the consideration of CO_2 consumption at various CO_2 inlet flowrates at 300 mA cm^{-2} (columns with dash line show the faradaic efficiency calculated without considering CO_2 consumption). (b) Overestimated C_2H_4 faradaic efficiency without the consideration of CO_2 consumption (left axis) as a function of CO_2 inlet flow and flow difference between CO_2 inlet and gas outlet (right axis). The overestimated values (left axis) were obtained by comparing C_2H_4 faradaic efficiency in dash lines and related solid lines in (a).

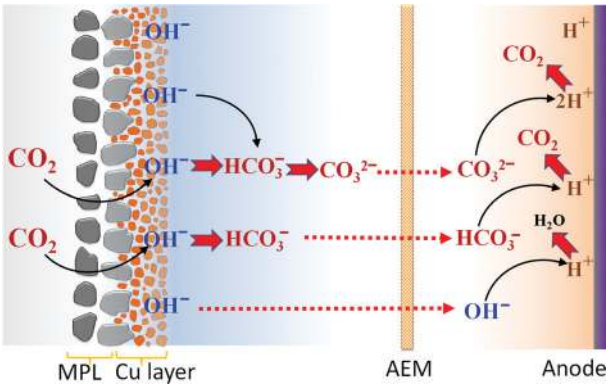

Scheme 1 Proposed carbon balance paths *via* CO_3^{2-} or HCO_3^- formation from CO_2 and a subsequent CO_2 evolution from CO_3^{2-} or HCO_3^- (red dash lines with arrows show the possible charge-carrying ionic species for AEM while using $KHCO_3$ electrolyte) in flow electrolyzers.

Interestingly, we found a near identical flow discrepancy between CO_2 inlet and gas outlet flowrates at different CO_2 inlet flow (Fig. 4b), which indicates that the nearly same CO_2 consumption rate occurred irrespective of CO_2 inlet flow. The nearly identical CO_2 consumption rate under different CO_2 inlet flow corresponds to the larger discrepancy in the faradaic efficiencies for gas products between corrected and uncorrected flow at lower CO_2 inlet flowrates (Fig. 4a). Of particular note, the faradaic efficiency for C_2H_4 was significantly overestimated from 7% to 28.6% with decreasing CO_2 inlet flow from 45 ml min^{-1} to 15 ml min^{-1} in 1 M KOH at 300 mA cm^{-2}. Based on eqn S16 (or eqn S17, ESI†), we found that the overestimation ratio for faradaic efficiencies of gas products enhanced from 15.7% to 64% with decreasing CO_2 inlet flow from 45 ml min^{-1} to 15 ml min^{-1} (Fig. S18, ESI†). In addition, the near constant CO_2 consumption rate may offer useful mass transfer information related to the gas diffusion layer and catalyst for future studies.

Captured CO_2 throughout the electrolyte

Based on the results of Fig. 1, high-rate CO_2 reduction leads to a substantial CO_2 consumption, thus it is pertinent to understand where all the CO_2 goes to achieve a complete carbon balance. With a near 100% faradaic efficiency toward all products, the total carbon in the form of all generated products is significantly less than that of total CO_2 consumption during CO_2 reduction electrolysis. In addition to CO_2 that was converted into products, the electrolyte is capable of capturing CO_2 as CO_3^{2-} or HCO_3^- (eqn (1) and (2)) at the electrode/electrolyte interface. In the case of 1 M $KHCO_3$ as an electrolyte, substantial additional carbonate or bicarbonate formed *via* capturing CO_2 could not exist in the electrolyte (due to charge balancing issues: total anion charge must equal total cation charge), thus there must be a CO_2 degassing mechanism through either the catholyte or anolyte. A test was employed in a closed-cycle catholyte with a vent for gases, and a volumetric flow meter showed no gas evolution from catholyte during the course of CO_2 reduction at 200 mA cm^{-2}. In contrast, we detected CO_2 evolution released from anolyte, accompanied with the anodically produced O_2 (using a setup shown in Fig. S8, ESI†).

To gain insights into capturing CO_2 in the catholyte and then releasing it in the anolyte, Scheme 1 shows a carbon balance path through a two-step procedure of CO_3^{2-} or HCO_3^- formation *via* capturing CO_2 at cathode/electrolyte interface and a subsequent CO_2 generation from CO_3^{2-} or HCO_3^- at the anode/electrolyte interface. In the cathodic reactions at high current densities in a $KHCO_3$ electrolyte, a substantial amount of OH^- generated near the catalyst surface will react with CO_2 to form CO_3^{2-} or HCO_3^- (eqn (1) and (2)), and then the anions including CO_3^{2-}, HCO_3^- or residual OH^- will transport from the catholyte to anolyte *via* AEM as charge-carriers. Meanwhile, the pH drops locally at the anode/anolyte interface due to H^+ generation by the water oxidation reaction, as below:

$$2H_2O \rightarrow O_2 + 4H^+ + 4e^- \quad (3)$$

Subsequently, CO_3^{2-}, HCO_3^- or OH^- coming from the catholyte will neutralize the H^+ (Scheme 1) generated near the anode surface owing to the following reactions:[43]

$$HCO_3^- + H^+ \rightarrow CO_2 + H_2O \quad (4)$$

$$CO_3^{2-} + 2H^+ \rightarrow CO_2 + H_2O \quad (5)$$

$$OH^- + H^+ \rightarrow H_2O \quad (6)$$

Thus, a low local pH will lead to CO_2 degassing in anolyte, which derives from the captured CO_2 by the reaction with OH^- in catholyte. After combining eqn (3) with the neutralization reactions (eqn (4)–(6)), we can get highly useful equations as follows:

$$4HCO_3^- \rightarrow 4CO_2 + O_2 + 2H_2O + 4e^- \quad (7)$$

$$2CO_3^{2-} \rightarrow 2CO_2 + O_2 + 4e^- \quad (8)$$

$$4OH^- \rightarrow 2H_2O + O_2 + 4e^- \quad (9)$$

From these simple modifications, it can be seen that the gas composition ratio of CO_2 to O_2 in the anolyte will be 4, 2 and 0 if the only charge-carrier for AEM is HCO_3^-, CO_3^{2-} or OH^-, respectively. Evidently, the main charge-carrying anion species through the AEM is not only linked to CO_2 generation rate, but

Published on 12 February 2020. Downloaded by DTU Library on 11/20/2020 11:30:33 AM.

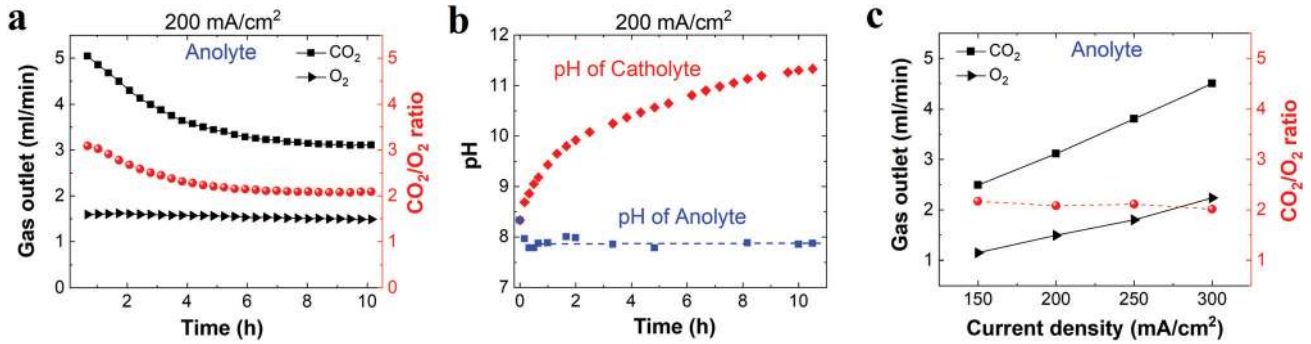

Fig. 5 (a) Flowrate of CO_2 and O_2 released from anolyte, and related CO_2/O_2 ratio during CO_2 reduction electrolysis at 200 mA cm^{-2}. (b) Electrolyte pH over CO_2 reduction electrolysis. (c) Flowrate of CO_2 and O_2 from anolyte as a function of current density at steady state. 1 M $KHCO_3$ was used in all these experiments as initial catholyte (50 ml) and anolyte (50 ml).

also likely represents the dominant anions in the catholyte. In addition, the conductivity of the membrane is also a function of ionic species.[44,45] Thus, it is highly crucial to identify whether HCO_3^-, CO_3^{2-} or potentially even OH^- is the dominant ion transferring across the AEM.

As presented in Fig. 5a, the composition ratio of CO_2/O_2 gradually decreased from ~3 to ~2 in the initial 4 h, and was then maintained at ~2 for the duration of electrolysis at 200 mA cm^{-2} in 1 M $KHCO_3$. This finding implies that the main transport charge-carrier for AEM quickly changed from a mixture of HCO_3^- and CO_3^{2-} to an almost pure CO_3^{2-} during the electrolysis, which can be attributed to the rapid transformation of HCO_3^- to CO_3^{2-} in the catholyte. By combining flow meter data with GC analysis (Fig. S8, ESI†), we found that the flowrate of anodic CO_2 decreased from ~5 ml min^{-1} to ~3 ml min^{-1} over an electrolysis experiment (Fig. 5a), which is consistent with the theoretical calculation of flowrates (3 ml min^{-1}) based on CO_3^{2-} serving as the main transport charge-carriers for AEM (Fig. S12, ESI†). At the same time, a constant O_2 flowrate with ~1.5 ml min^{-1} was observed during the electrolysis (Fig. 5a), which is in line with theoretically calculated O_2 flowrates (Fig. S12, ESI†).

To provide additional evidence of the anion species transformation in the electrolyte, the pH of the electrolyte was also measured over the course of an electrolysis experiment. Fig. 5b shows that the anolyte pH reduced to ~7.9 within 10 min and then maintained at that pH throughout the rest of electrolysis experiment, thus allowing for the release of CO_2 into the anolyte. In contrast, the catholyte pH increased sharply initially, and then approached > 11 after 7 h (Fig. 5b), which further confirms that the bicarbonate catholyte rapidly transformed to a carbonate catholyte (pH of 1 M $KHCO_3$ is 8.3; pH of 0.5 M K_2CO_3 is 11.6). Of particular note, the quickly increasing catholyte pH in the initial CO_2 reduction experiment reveals that at high-rate CO_2 reduction, a pH-independent reference such as a standard hydrogen electrode (SHE) is more suitable for reporting applied potentials than a pH-dependent reversible hydrogen electrode (RHE).

To understand the effect of current on the main transport charge-carriers, an analysis of gas released from the anolyte was also performed at 150, 250 and 300 mA cm^{-2} (Fig. S9, ESI†). After the system approximately reached steady state during 10 h electrolysis, the ratio of CO_2/O_2 and the corresponding flowrates of CO_2 and O_2 were plotted in Fig. 5c, indicating that CO_3^{2-} was the main transport charge-carriers. This figure also shows this effect is independent of current (for conditions ≥150 mA cm^{-2}). However, the catholyte transition rate from bicarbonate to carbonate was faster at higher current densities (Fig. S10, ESI†), due to current-dependent OH^- generation rate *via* cathodic reactions.

When 1 M KOH was used as an electrolyte in both anolyte (20 ml reservoir) and catholyte (20 ml reservoir), analysis of the gas from the anolyte over time (Fig. 6) shows that no CO_2 was detected during the initial 2.5 h, which can be attributed to remaining KOH in anolyte, which prevented CO_2 from existing (CO_2 cannot exist in alkaline solutions). After 2.5 h, CO_2 started to evolve and then rapidly reached a CO_2/O_2 ratio of 2. Subsequently, the stable CO_2/O_2 ratio of 2 and the constant CO_2 flowrate of ~3 ml min^{-1} were observed after 3.5 h, which means that the transport of charge-carrier for AEM is CO_3^{2-} (Fig. 6). In addition, after 5 h we found that the pH of catholyte and anolyte was reduced from 13.6 to ~11.6 and ~8, respectively (pH of 0.5 M K_2CO_3 is 11.6). These observations indicate that the CO_2 was captured in KOH at the catholyte, gradually

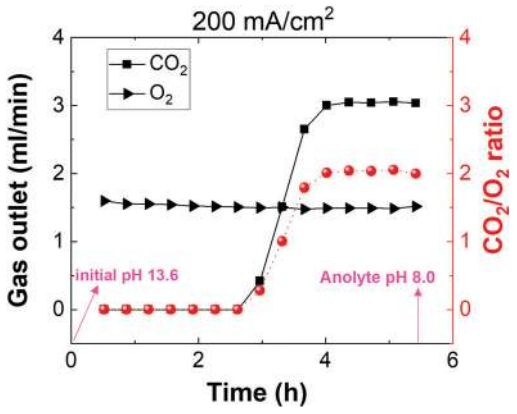

Fig. 6 The flowrate of O_2 and CO_2 released from anolyte and the related CO_2/O_2 ratio over CO_2 reduction electrolysis in 1 M KOH at 200 mA cm^{-2} (each bottle was filled with 20 ml of 1 M KOH as initial catholyte and anolyte).

 This journal is © The Royal Society of Chemistry 2020

Published on 12 February 2020. Downloaded by DTU Library on 11/20/2020 11:30:33 AM.

converting OH^- to CO_3^{2-} (KOH electrolyte transformed to K_2CO_3), which then transported to the anolyte through the AEM. Meanwhile, the existing KOH in the anolyte was neutralized by H^+ produced in the anodic reaction (eqn (3)), thus slowly decreasing the anolyte pH. After reaching a near neutral anolyte, CO_2 was released *via* the reaction of carbonate with H^+ at the anode/electrolyte interface (Scheme 1). In addition, a part of carrier ions *via* AEM should be carbonate (the rest is OH^-) in basic solutions in the initial 2.5 h, which leads to a large amount of existing CO_3^{2-} in anolyte before releasing CO_2, thus quickly allowing the system to reach a CO_2/O_2 ratio of 2 once a neutral anolyte was reached. Interestingly, all the above results show that no mater whether $KHCO_3$ or KOH was used as the initial electrolyte for high-rate CO_2 reduction, both of them transformed to K_2CO_3 as the final catholyte after long-term electrolysis experiments.

It should be noted that by increasing the anolyte and catholyte volume to 50 ml of 1 M KOH, no CO_2 evolution was detected during a 6 hour test (Fig. S11, ESI†). These experiments demonstrate the large capacity of KOH to capture CO_2 and reiterates the point that it is essential to understand the complete carbon balance to accurately analyze CO_2 reduction.

Carbon balance and implications

Based on the aforementioned discussion, eventually the carbon from CO_2 inlet flow must be balanced with carbonate formation, product generation and outgoing CO_2. In the case of 1 M $KHCO_3$ as an electrolyte, the final carbon balance (eqn S14, ESI†) in Fig. 7a shows that (i) the unreacted CO_2 flowrate (residual CO_2) after the reactor, (ii) the consumed CO_2 flowrate for carbonate formation (reaction with OH^-) and (iii) consumed CO_2 flowrate for the conversation into products added up to a total of $\sim$45 ml min^{-1} at various current densities, which is equal to CO_2 inlet flowrate used in these experiments. In addition, the total CO_2 consumption rate (carbonate formation and product generation) increased as the current densities enhanced (Fig. 7a), which is consistent with the lower outlet flowrates for the cathode gas at higher current densities observed in Fig. 1b. Notably, only $\sim$30% of the CO_2 consumption was involved in CO_2 reduction for product formation, whereas most of consumed CO_2 (70%) was captured by the electrolyte to form carbonate (Fig. 7b).

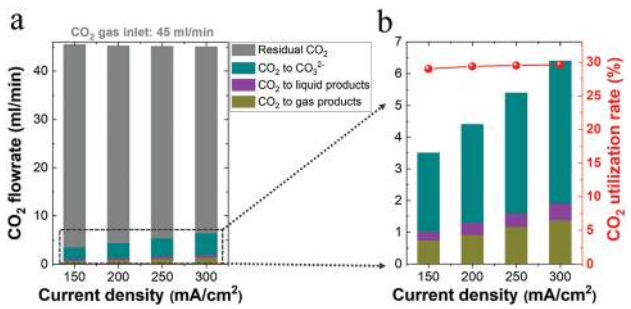

Fig. 7 (a) Carbon balance for CO_2 reduction in 1 M $KHCO_3$. The total consumed CO_2 flow for carbonate formation and CO_2 reduction to all liquid and gas products as well as residual (*i.e.* unused) CO_2 flow were considered. (b) Ratio of CO_2 used in products formation to total CO_2 consumption (right axis).

In addition, Fig. 7b indicates that the CO_2 utilization rate (ratio of CO_2 converted into products *versus* total CO_2 consumption) is nearly independent of the total CO_2 consumption rate at different current densities since the catalytic selectivity is roughly same (Fig. 3a).

The carbon balance was also roughly calculated for high-rate CO_2 reduction in 1 M KOH (Table S2, ESI†), which shows a higher CO_2 consumption rate *via* reaction with OH^- (forming carbonate) compared to that of 1 M $KHCO_3$ (Table S1, ESI†). Thus, with roughly identical catalytic selectivity (Fig. 3), the higher CO_2 capture rate in 1 M KOH correspondingly leads to a lower CO_2 utilization rate (24–26% in Table S2, ESI†) in comparison with that of 1 M $KHCO_3$. Obviously, in 5 M KOH electrolyte (highly concentrated alkaline), consumed CO_2 to carbonate formation would be expected to be much higher than those in 1 M KOH and 1 M $KHCO_3$, due to the fact that KOH acts as a reservoir for capturing CO_2.

Implications of CO_2 crossover and emission from the anolyte

From a fundamental standpoint, the relatively consistent CO_2 to O_2 ratio of 2 shown in this study indicates that for every 4 electrons (*i.e.* O_2 evolution is a $4e^-$ process) transferred in the circuit, 2 carbonates transfer through the membrane and are degassed out of the anolyte as 2 CO_2 molecules. The CO_2 reduction to ethylene or ethanol is a 12-electron transfer process, thus every 1 molecule of ethanol or ethylene formation should theoretically correspond to 6 CO_2's degassing through the anolyte. If a reactor is built with 100% ethylene or ethanol selectivity, 75% of all CO_2 consumed by the reactor should be emitted in the anolyte, since both ethanol and ethylene are two-carbon products. Additionally, CO_2 reduction to CO requires a 2-electron transfer, and CO is only a one-carbon product, which entails that 50% of all CO_2 consumed in the reactor should be emitted out of the anolyte if CO selectivity is 100%. Fig. 7 presents that 70% CO_2 consumption was emitted out of the anolyte, which is well in line with the product distribution shown in Fig. 3.

To put these emissions into perspective, ethylene produced *via* fossil based sources give off 0.71–0.92 kg CO_2 per kg of ethylene,[46] whereas even if the approach here yielded pure ethylene (100% selectivity), the high theoretical CO_2 crossover to the anolyte (75% by mole) would result in CO_2 emissions of 9.4 kg per kg ethylene formation. Thereby, to be environmentally successful in this process, the CO_2 released in anolyte would require to be captured and recycled, or a new approach needs to be developed to mitigate CO_2 crossover.

There have been a significant amount of techno-economic analysis done for electrochemical CO_2 reduction to products such as ethylene, and if aggressive parameters are used, CO_2 reduction to products could be profitable.[47–50] However, these models have not considered CO_2 emission and capture in the anolyte. Various models for CO_2 capture from concentrated CO_2 sources range from $\sim$20–100 $ per ton CO_2.[51–53] Capturing and recycling the CO_2 from the anolyte may be on the lower side of this range because the CO_2 concentration in the flue gas is already very high (CO_2 content is $\sim$66.7% by mole), and oxygen

Published on 12 February 2020. Downloaded by DTU Library on 11/20/2020 11:30:33 AM.

is the only species that needs to be removed. Nevertheless, if approximately 9.4 kg of CO_2 needs to be recycled for every kg of ethylene produced, this CO_2 emission and capture in the anolyte could have a significant effect on the economic potential for this approach (current ethylene prices around 800–1100 $ per ton [54,55]). While a full techno-economic analysis is beyond the scope of this work, the aforementioned discussion highlights the importance of understanding and trying to mitigate CO_2 crossover to the anolyte.

An alternative approach to help resolve this issue would be to break the reaction into an initial conversion of CO_2 to CO and a following reduction of CO to highly valuable multi-carbon products.[27] In this two-step cascade reaction process, while the initial two-electron transfer for CO_2 reduction to CO still would struggle with CO_2 crossover, CO does not form a carbonate (no carbon source crossover) in the subsequent CO reduction, thus overall CO_2 crossover will be significantly reduced. The full analysis of CO reduction will be investigated in a further work.

Conclusions

In conclusion, our results show that the CO_2 consumption *via* the reaction with OH^- in flow electrolyzers could significantly reduce the flowrate of gas outlet, which is closely linked to the final evaluation of the catalytic selectivity for gas products. We found the discrepancy of 5.9%, 7% and 12% for C_2H_4 faradaic efficiency with and without the consideration of CO_2 consumption at 300 mA cm^{-2} in 1 M $KHCO_3$, 1 M KOH and 5 M KOH, respectively with a 45 ml min^{-1} CO_2 inlet flow rate. Furthermore, we found C_2H_4 faradaic efficiency was significantly overestimated from 7% to 28.6% when CO_2 inlet flow decreased from 45 ml min^{-1} to 15 ml min^{-1} in 1 M KOH at 300 mA cm^{-2}, corresponding to an overestimation ratio of faradaic efficiencies from 15.7% to 64%.

According to a carbon balance path, the gases released from the anolyte was examined during CO_2 reduction, suggesting a rapid transformation of the electrolyte, which is consistent with a variation of electrolyte pH. We found that most of the consumed CO_2 ($\sim$70%) at high current density CO_2 reduction (for 1 M $KHCO_3$) was absorbed by the electrolyte to form carbonate. In addition, 8 different liquid products were detected, accompanied by a significant amount of formate and acetate crossover through the anion exchange membrane. This study presents that CO_2 consumption should be taken into account for evaluating catalytic selectivity of gas products, and both catholyte and anolyte should be analyzed for liquid products, thus enabling one to obtain reliable results for high-rate CO_2 reduction.

Conflicts of interest

There are no conflicts to declare.

Acknowledgements

This work was supported by the Villum Foundation V-SUSTAIN grant 9455 to the Villum Center for the Science of Sustainable Fuels and Chemicals. This work was also supported by ECOEthylene project from the Innovation Fund Denmark (Grant# 8057-00018B).

Notes and references

1 D. T. Whipple and P. J. A. Kenis, *J. Phys. Chem. Lett.*, 2010, **1**, 3451–3458.
2 Z. W. Seh, J. Kibsgaard, C. F. Dickens, I. B. Chorkendorff, J. K. Norskov and T. F. Jaramillo, *Science*, 2017, **355**, eaad4998.
3 C. W. Li, J. Ciston and M. W. Kanan, *Nature*, 2014, **508**, 504–507.
4 J. Qiao, Y. Liu, F. Hong and J. Zhang, *Chem. Soc. Rev.*, 2014, **43**, 631–675.
5 M. Ma, K. Djanashvili and W. A. Smith, *Angew. Chem., Int. Ed.*, 2016, **55**, 6680–6684.
6 D. D. Zhu, J. L. Liu and S. Z. Qiao, *Adv. Mater.*, 2016, **28**, 3423–3452.
7 M. G. Kibria, J. P. Edwards, C. M. Gabardo, C. T. Dinh, A. Seifitokaldani, D. Sinton and E. H. Sargent, *Adv. Mater.*, 2019, **31**, 1807166.
8 K. Jiang, R. B. Sandberg, A. J. Akey, X. Y. Liu, D. C. Bell, J. K. Norskov, K. R. Chan and H. T. Wang, *Nat. Catal.*, 2018, **1**, 111–119.
9 Y. H. Chen, C. W. Li and M. W. Kanan, *J. Am. Chem. Soc.*, 2012, **134**, 19969–19972.
10 K. P. Kuhl, E. R. Cave, D. N. Abram and T. F. Jaramillo, *Energy Environ. Sci.*, 2012, **5**, 7050–7059.
11 R. Kas, K. K. Hummadi, R. Kortlever, P. de Wit, A. Milbrat, M. W. J. Luiten-Olieman, N. E. Benes, M. T. M. Koper and G. Mul, *Nat. Commun.*, 2016, **7**, 10748.
12 N. Kornienko, Y. B. Zhao, C. S. Kiley, C. H. Zhu, D. Kim, S. Lin, C. J. Chang, O. M. Yaghi and P. D. Yang, *J. Am. Chem. Soc.*, 2015, **137**, 14129–14135.
13 M. Liu, Y. J. Pang, B. Zhang, P. De Luna, O. Voznyy, J. X. Xu, X. L. Zheng, C. T. Dinh, F. J. Fan, C. H. Cao, F. P. G. de Arquer, T. S. Safaei, A. Mepham, A. Klinkova, E. Kumacheva, T. Filleter, D. Sinton, S. O. Kelley and E. H. Sargent, *Nature*, 2016, **537**, 382–386.
14 M. Ma, K. Liu, J. Shen, R. Kas and W. A. Smith, *ACS Energy Lett.*, 2018, **3**, 1301–1306.
15 M. Ma, H. A. Hansen, M. Valenti, Z. Wang, A. P. Cao, M. D. Dong and W. A. Smith, *Nano Energy*, 2017, **42**, 51–57.
16 Y. Hori, I. Takahashi, O. Koga and N. Hoshi, *J. Phys. Chem. B*, 2002, **106**, 15–17.
17 K. J. P. Schouten, Z. S. Qin, E. P. Gallent and M. T. M. Koper, *J. Am. Chem. Soc.*, 2012, **134**, 9864–9867.
18 H. Mistry, A. S. Varela, C. S. Bonifacio, I. Zegkinoglou, I. Sinev, Y. W. Choi, K. Kisslinger, E. A. Stach, J. C. Yang, P. Strasser and B. R. Cuenya, *Nat. Commun.*, 2016, **7**, 12123.
19 T. Burdyny and W. A. Smith, *Energy Environ. Sci.*, 2019, **12**, 1442–1453.
20 L. C. Weng, A. T. Bell and A. Z. Weber, *Phys. Chem. Chem. Phys.*, 2018, **20**, 16973–16984.
21 C. T. Dinh, T. Burdyny, M. G. Kibria, A. Seifitokaldani, C. M. Gabardo, F. P. G. de Arquer, A. Kiani, J. P. Edwards,

 This journal is © The Royal Society of Chemistry 2020

Published on 12 February 2020. Downloaded by DTU Library on 11/20/2020 11:30:33 AM.

P. De Luna, O. S. Bushuyev, C. Q. Zou, R. Quintero-Bermudez, Y. J. Pang, D. Sinton and E. H. Sargent, *Science*, 2018, **360**, 783–787.

22 T. Moller, W. Ju, A. Bagger, X. L. Wang, F. Luo, T. N. Thanh, A. S. Varela, J. Rossmeisl and P. Strasser, *Energy Environ. Sci.*, 2019, **12**, 640–647.

23 M. G. Kibria, C. T. Dinh, A. Seifitokaldani, P. De Luna, T. Burdyny, R. Quintero-Bermudez, M. B. Ross, O. S. Bushuyev, F. P. G. D. Arguer, P. D. Yang, D. Sinton and E. H. Sargen, *Adv. Mater.*, 2018, **30**, 1804867.

24 C. T. Dinh, F. P. G. de Arquer, D. Sinton and E. H. Sargent, *ACS Energy Lett.*, 2018, **3**, 2835–2840.

25 S. Verma, X. Lu, S. C. Ma, R. I. Masel and P. J. A. Kenis, *Phys. Chem. Chem. Phys.*, 2016, **18**, 7075–7084.

26 B. Endrodi, G. Bencsik, F. Darvas, R. Jones, K. Rajeshwar and C. Janaky, *Prog. Energy Combust. Sci.*, 2017, **62**, 133–154.

27 M. Jouny, W. Luc and F. Jiao, *Nat. Catal.*, 2018, **1**, 748–755.

28 T. T. H. Hoang, S. Verma, S. C. Ma, T. T. Fister, J. Timoshenko, A. I. Frenkel, P. J. A. Kenis and A. A. Gewirth, *J. Am. Chem. Soc.*, 2018, **140**, 5791–5797.

29 B. Kim, F. Hillman, M. Ariyoshi, S. Fujikawa and P. J. A. Kenis, *J. Power Sources*, 2016, **312**, 192–198.

30 C. M. Gabardo, A. Seifitokaldani, J. P. Edwards, C. T. Dinh, T. Burdyny, M. G. Kibria, C. P. O'Brien, E. H. Sargent and D. Sinton, *Energy Environ. Sci.*, 2018, **11**, 2531–2539.

31 S. Ma, M. Sadakiyo, M. Heima, R. Luo, R. T. Haasch, J. I. Gold, M. Yamauchi and P. J. A. Kenis, *J. Am. Chem. Soc.*, 2017, **139**, 47–50.

32 P. De Luna, R. Quintero-Bermudez, C. T. Dinh, M. B. Ross, O. S. Bushuyev, P. Todorovic, T. Regier, S. O. Kelley, P. D. Yang and E. H. Sargent, *Nat. Catal.*, 2018, **1**, 103–110.

33 J. J. Lv, M. Jouny, W. Luc, W. L. Zhu, J. J. Zhu and F. Jiao, *Adv. Mater.*, 2018, **30**, 1803111.

34 W. Luc, B. H. Ko, S. Kattel, S. Li, D. Su, J. G. G. Chen and F. Jiao, *J. Am. Chem. Soc.*, 2019, **141**, 9902–9909.

35 S. Verma, Y. Hamasaki, C. Kim, W. X. Huang, S. Lu, H. R. M. Jhong, A. A. Gewirth, T. Fujigaya, N. Nakashima and P. J. A. Kenis, *ACS Energy Lett.*, 2018, **3**, 193–198.

36 R. M. Wang, H. Haspel, A. Pustovarenko, A. Dikhtiarenko, A. Russkikh, G. Shterk, D. Osadchii, S. Ould-Chikh, M. Ma, W. A. Smith, K. Takanabe, F. Kapteijn and J. Gascon, *ACS Energy Lett.*, 2019, **4**, 2024–2031.

37 Y. G. C. Li, D. K. Zhou, Z. F. Yan, R. H. Goncalves, D. A. Salvatore, C. P. Berlinguette and T. E. Mallouk, *ACS Energy Lett.*, 2016, **1**, 1149–1153.

38 G. Larrazabal, P. Strøm-Hansen, J. P. Heli, K. Zeiter, K. T. Therkildsen, I. Chorkendorff and B. Seger, *ACS Appl. Mater. Interfaces*, 2019, **11**, 41281–41288.

39 Y. A. Lebedev, Y. M. Korolev, V. M. Polikarpov, L. N. Ignat'eva and E. M. Antipov, *Crystallogr. Rep.*, 2010, **55**, 609–614.

40 Y. Hori, R. Takahashi, Y. Yoshinami and A. Murata, *J. Phys. Chem. B*, 1997, **101**, 7075–7081.

41 Y. G. C. Li, Z. F. Yan, J. Hitt, R. Wycisk, P. N. Pintauro and T. E. Mallouk, *Adv. Sustainable Syst.*, 2018, **2**, 1700187.

42 E. L. Clark and A. T. Bell, *J. Am. Chem. Soc.*, 2018, **140**, 7012–7020.

43 H. Zhong, K. Fujii, Y. Nakano and F. M. Jin, *J. Phys. Chem. C*, 2015, **119**, 55–61.

44 J. R. Varcoe, P. Atanassov, D. R. Dekel, A. M. Herring, M. A. Hickner, P. A. Kohl, A. R. Kucernak, W. E. Mustain, K. Nijmeijer, K. Scott, T. W. Xu and L. Zhuang, *Energy Environ. Sci.*, 2014, **7**, 3135–3191.

45 O. I. Deavin, S. Murphy, A. L. Ong, S. D. Poynton, R. Zeng, H. Herman and J. R. Varcoe, *Energy Environ. Sci.*, 2012, **5**, 8584–8597.

46 M. Patel, *Energy*, 2003, **28**, 721–740.

47 S. Verma, B. Kim, H. Jhong, S. C. Ma and P. J. A. Kenis, *ChemSusChem*, 2016, **9**, 1972–1979.

48 M. Jouny, W. Luc and F. Jiao, *Ind. Eng. Chem. Res.*, 2018, **57**, 2165–2177.

49 O. S. Bushuyev, P. De Luna, C. T. Dinh, L. Tao, G. Saur, J. van de Lagemaat, S. O. Kelley and E. H. Sargent, *Joule*, 2018, **2**, 825–832.

50 P. De Luna, C. Hahn, D. Higgins, S. A. Jaffer, T. F. Jaramillo and E. H. Sargent, *Science*, 2019, **364**, eaav3506.

51 H. Naims, *Environ. Sci. Pollut. Res.*, 2016, **23**, 22226–22241.

52 L. Irlam, *Global costs of carbon capture and storage—2017 update*, Melbourne, Australia, 2017.

53 J. Deutch, S. Benson, R. Bras, E. Carter, A. Majumdar, D. Ort, M. Ramage, R. Socolow, E. Toone, G. Whitesides and M. Wrighton, *Task Force on RD&D Strategy for CO_2 Utilization and/or Negative Emissions at the gigatonne scale*, 2016.

54 A. Boulamanti and J. A. Moya, *Renewable Sustainable Energy Rev.*, 2017, **68**, 1205–1212.

55 C. Chen, J. F. K. Kotyk and S. W. Sheehan, *Chem*, 2018, **4**, 2571–2586.